Current-Voltage and Floating-Potential characteristics of cylindrical emissive probes from a full-kinetic model based on the orbital motion theory

Xin Chen[1] and Gonzalo Sánchez-Arriaga[2]

[1 2] Bioengineering and Aerospace Engineering Department, Universidad Carlos III de Madrid, Avd. de la Universidad 30 28911, Leganés (Madrid), Spain

E-mail: [1]xin.chen@uc3m.es

E-mail: [2]gonzalo.sanchez@uc3m.es

Abstract. To model the sheath structure around an emissive probe with cylindrical geometry, the Orbital-Motion theory takes advantage of three conserved quantities (distribution function, transverse energy, and angular momentum) to transform the stationary Vlasov-Poisson system into a single integro-differential equation. For a stationary collisionless unmagnetized plasma, this equation describes self-consistently the probe characteristics. By solving such an equation numerically, parametric analyses for the current-voltage (IV) and floating-potential (FP) characteristics can be performed, which show that: (a) for strong emission, the space-charge effects increase with probe radius; (b) the probe can float at a positive potential relative to the plasma; (c) a smaller probe radius is preferred for the FP method to determine the plasma potential; (d) the work function of the emitting material and the plasma-ion properties do not influence the reliability of the floating-potential method. Analytical analysis demonstrates that the inflection point of an IV curve for non-emitting probes occurs at the plasma potential. The flat potential is not a self-consistent solution for emissive probes.

1. Introduction

Plasma potential is one of the principal parameters to be measured for understanding a wide range of plasma phenomena. For this purpose, emissive probes (EPs) are frequently used, mainly due to their simple practical implementation and robustness [1][2]. The determination of plasma potential relies on two experimental curves of EP measurements: the current-voltage (IV) characteristics and the floating-potential (FP) characteristics. When the EP is heated to emit thermionic electrons and thus to achieve certain emission level, the current-voltage characteristic is obtained by measuring the net current to the probe, for a range of different probe biases. The floating-potential characteristic is obtained by directly measuring the probe bias at the floating condition (i.e., zero net current), for different emission levels.

Theoretical difficulties for EPs arise from the cylindrical geometry and the space-charge effects that can result in a virtual cathode in front of the probe (i.e., non-monotonic potential profile). Available theoretical works commonly considered planar geometry [3][4][5]. The effects of the particle orbital motions were neglected [6], or partially developed in some asymptotic regimes and limited conditions [7][8]. Not until recently, a full-kinetic model based on the Orbital-Motion Theory (OMT) for cylindrical EPs was finally developed [9]. This work is organized as

follows. In Sec. 2, the model in [9] is briefly described, with focus on the independent parameters that determine the EP characteristics. Parametric studies on the current-voltage and floating-potential characteristics are presented in Sec. 3 and Sec. 4, respectively, together with discussions on their applications. The conclusions are summarized in Sec. 5.

2. OMT for cylindrical emitters

2.1. Plasma and probe conditions

Let us consider a long emissive probe (denoted by the subscript p), with two-dimensional cylindrical geometry, radius R_p, and bias ϕ_p relative to the Maxwellian plasma at infinity that has unperturbed density N_∞, electron temperature T_e, ion temperature T_i, and ion mass m_i. As long as collisions, plasma drift, particle trapping, transient effects, and magnetic field are not significant, the OMT can be applied to model the probe-plasma interaction.

Thermionic electrons are emitted at the probe with a half-Maxwellian (HM) distribution based on the probe temperature (T_p) [10]. The thermionic current density is given by the Richardson-Dushman (RD) law as

$$J_{RD} = \lambda_{RD} A_0 {T_p}^2 \exp\left(-\frac{eW}{k_B T_p}\right) , \tag{1}$$

with W the work function in eV, T_p the probe temperature in K, λ_{RD} the material-specific correction factor, e the elementary charge, and A_0 a universal constant given by

$$A_0 \equiv \frac{4\pi e m_e k_B^2}{h^3} \approx 1.20173 \times 10^6 \,\mathrm{A\,m^{-2}\,K^{-2}} , \tag{2}$$

where m_e is the electron mass, k_B is the Boltzmann constant, and h is the Plank constant. Combing the HM distribution and the RD law, electrons are emitted at the probe with a density

$$\begin{aligned} N_{emp}(\lambda_{RD}, T_p, W) &= \sqrt{\frac{\pi m_e}{2 k_B T_p}} \frac{\lambda_{RD} A_0 T_p^2}{e} \exp\left(-\frac{eW}{k_B T_p}\right) \\ &= \lambda_{RD} \left(\frac{2\pi m_e k_B T_p}{h^2}\right)^{3/2} \exp\left(-\frac{eW}{k_B T_p}\right) . \end{aligned} \tag{3}$$

The dimensional parameters that determine the net current to probe are: plasma properties (T_e, T_i, m_i, and N_∞), thermionic properties of the probe (T_p, W, and λ_{RD}), and the probe geometry R_p and bias ϕ_p.

2.2. The Vlasov-Poisson system

To obtain the net current, one needs to first find out the potential distribution along the radial direction of the probe, by solving the Vlasov-Poisson system self-consistently. The dimensionless radial coordinate r is defined as the radial distance to the cylinder axis normalized by R_p. The r-dependent electric potential and particle densities are normalized as

$$\varphi(r) \equiv \frac{e\phi}{k_B T_e} , \; n_{i,e}(r) \equiv \frac{N_{i,e}}{N_\infty} , \; n_{em}(r) \equiv \frac{N_{em}}{N_{emp}} , \tag{4}$$

with the subscript $\alpha = i, e, em$ denoting for plasma ion, plasma electron, and emitted electrons, respectively. Poisson's equation for cylindrical geometry then reads

$$\frac{1}{r}\frac{\mathrm{d}}{\mathrm{d}r}\left(r\frac{\mathrm{d}\varphi}{\mathrm{d}r}\right) = -\rho_p^2 \left(n_i - n_e - \beta n_{em}\right) , \quad \varphi(r=1) = \varphi_p , \quad \varphi(r\to\infty) \to 0 , \tag{5}$$

where ions are taken as single-charged, ρ_p is the radius to Debye length ratio

$$\rho_p \equiv \frac{R_p}{\lambda_{De}} \equiv \frac{R_p}{\sqrt{\varepsilon_0 k_B T_e / e^2 N_\infty}} \ , \tag{6}$$

and β is the emission level

$$\beta \equiv \frac{N_{emp}}{N_\infty} = \left(\frac{\delta_p}{\delta_s}\right)^{3/2} \exp\left(-\frac{\delta_w}{\delta_p}\right) \ , \ \delta_w \equiv \frac{eW}{k_B T_e} \ , \ \delta_s \equiv \frac{h^2 N_\infty^{2/3}}{2{\lambda_{RD}}^{2/3} \pi m_e k_B T_e} \ , \ \delta_p \equiv \frac{T_p}{T_e} \ . \tag{7}$$

Based on the OMT, the densities n_α on the right-hand-side of Poisson's equation can be written out explicitly as a function of $\varphi(r)$ according to Vlasov characteristics [9] [11]. The Vlasov-Poisson system then becomes a single integro-differential equation that is to be solved for $\varphi(r)$.

The particle density n_α at any radius r can be found by integrating the local distribution function f_α over the (v_r, v_θ) velocity space,

$$n_\alpha(r) = \int\int f_\alpha \left(r, v_r, v_\theta\right) \, \mathrm{d}v_r \, \mathrm{d}v_\theta \ , \tag{8}$$

where the normalizations applied are $2k_B T_\alpha f_\alpha / (m_\alpha N_{\infty,emp}) \rightarrow f_\alpha$ for distribution function, $\sqrt{m_\alpha / 2k_B T_\alpha} v_r \rightarrow v_r$ for radial velocity (positive outwards), and $\sqrt{m_\alpha / 2k_B T_\alpha} v_\theta \rightarrow v_\theta$ for azimuthal velocity. The Vlasov equation conserves the distribution function along particle orbits. Due to the Maxwellian plasma faraway from the probe and the HM electrons emitted at the probe, the local distributions for the particles existing at r are

$$f_\alpha(r, v_r, v_\theta) = H_\alpha \exp\left(-{v_r}^2 - {v_\theta}^2 - u_{\alpha r}\right) / \pi \ , \quad H_{i,e} = 1 \ , \quad H_{em} = 2 \ , \tag{9}$$

with the normalized *electric potential energy* $u_{\alpha r}(r)$ being defined for each species as

$$u_{er}(r) \equiv -\varphi(r), \quad u_{ir}(r) \equiv \frac{\varphi(r)}{\delta_i} \equiv \frac{\varphi(r)}{T_i / T_e} \ , \quad u_{emr}(r) \equiv \frac{\varphi_p - \varphi(r)}{\delta_p} \ . \tag{10}$$

For each specie, this electric potential energy is taken relative to the *origin* of the particle (infinity for $\alpha = i, e$ and probe for $\alpha = em$).

Due to the cylindrical symmetry of the problem and its stationary character, the normalized *angular momentum* and the normalized *transverse total energy*,

$$l_\alpha \equiv r v_\theta, \quad \epsilon_\alpha \equiv v_r^2 + v_\theta^2 + u_{\alpha r} \ , \tag{11}$$

are also conserved along particle orbits. They not only suffice to *characterize* the orbits but also allow transforming the density integration over the $v_r v_\theta$-space to the ϵl-space. After applying change of variables $(v_r, v_\theta) \rightarrow (\epsilon_\alpha, l_\alpha)$, Eq. (8) becomes

$$n_\alpha(r) = \int\int_{2D_r} \frac{f_\alpha \left(r, v_r, v_\theta\right)}{2\sqrt{l_{\alpha r}^2(r, \epsilon_\alpha) - l_\alpha^2}} \, \mathrm{d}\epsilon_\alpha \, \mathrm{d}l_\alpha \ , \tag{12}$$

$$l_{\alpha r}^2(r, \epsilon_\alpha) \equiv {l_\alpha}^2 + r^2 v_r^2 = r^2 \left(\epsilon_\alpha - u_{\alpha r}\right) \ . \tag{13}$$

The domain of integration $(2D_r)$ should contain all the values of the orbital invariants $(\epsilon_\alpha, l_\alpha)$ for the particles present at r, with the factor 2 for considering only positive l_α and $l_{\alpha r}$ hereafter.

For each species, without trapped particles, the r-dependent domain D_r is composed by two sub-domains, $D_r = D_{1r} + D_{2r}$: 1) The sub-domain D_{1r} stands for the particles that are able to overcome all the barriers to arrive at r for the first time; 2) the other sub-domain D_{2r} stands

for the particles that are reflected back to r and appear at that radius for the second time. For plasma species, D_{1r} and D_{2r} corresponds to *incoming* and *outgoing* particles, respectively (vice versa for emitted electrons).

According to Eq. (13), a particle is certainly *forbidden* at r if ${v_r}^2 > 0$ can not be satisfied. Consequently, for a particle to exist at r, it is *necessary* (but not *sufficient*) to have: a) an adequately large energy as $\epsilon_\alpha \geq u_{\alpha r}(r)$; b) for any energy in this range, a small enough angular momentum as $l_\alpha \leq l_{\alpha r}(r, \epsilon_\alpha)$. If the orbital characteristics (ϵ and l) of a particle can fulfil the *necessary* condition at any r' that is between r and the *origin* of the particle, this particle can arrive at r for the *first* time, thus yielding the D_{1r} domain as

$$\begin{gathered} D_{1r} = \{(\epsilon_\alpha, l_\alpha) : \epsilon_\alpha \geq u^*_{\alpha r}(r),\, l_\alpha \leq l^*_{\alpha r}(r, \epsilon_\alpha)\} \ , \\ u^*_{\alpha r}(r) \equiv \max_{r' \in S_r} u_\alpha(r') \ , \ l^*_{\alpha r}(r, \epsilon_\alpha) \equiv \min_{r' \in S_r} l_{\alpha r}(r', \epsilon_\alpha) \ , \\ S_r = \{1 \leq r' \leq r \text{ for } \alpha = em \ , \ r \leq r' < \infty \text{ for } \alpha = i, e\} \ . \end{gathered} \tag{14}$$

Among the particles within this D_{1r} domain, some plasma particles (emitted electrons) can be *captured* by the probe (infinity). The ϵl-domain that contains all the *captured* particles is thus

$$\begin{gathered} D_0 = \{(\epsilon_\alpha, l_\alpha) : \epsilon_\alpha \geq u^*_\alpha,\, l_\alpha \leq l^*_\alpha(\epsilon_\alpha)\} \ , \\ u^*_\alpha \equiv \max_{r' \in S} u_\alpha(r') \ , \quad l^*_\alpha(\epsilon_\alpha) \equiv \min_{r' \in S} l_{\alpha r}(r', \epsilon_\alpha) \ , \quad S = \{\, 1 \leq r' < \infty\} \ . \end{gathered} \tag{15}$$

Readily, the *reflected* sub-domain D_{2r} can be found as the relative complement of D_0 in D_{1r}, i.e., $D_{2r} = D_{1r} - D_0$.

After substituting $D_{2r} = D_{1r} - D_0$ into Eq. (12) and using Eqs. (14) and (15), the particle density becomes

$$n_\alpha(r) = \frac{2H_\alpha}{\pi} \int_{u^*_{\alpha r}(r)}^{\infty} \exp(-\epsilon_\alpha) \arcsin \frac{l^*_{\alpha r}(r, \epsilon_\alpha)}{l_{\alpha r}(r, \epsilon_\alpha)} \, \mathrm{d}\epsilon_\alpha - \frac{H_\alpha}{\pi} \int_{u^*_\alpha}^{\infty} \exp(-\epsilon_\alpha) \arcsin \frac{l^*_\alpha(\epsilon_\alpha)}{l_{\alpha r}(r, \epsilon_\alpha)} \, \mathrm{d}\epsilon_\alpha \ . \tag{16}$$

Such an integration does not only depend on the value of $\varphi(r)$ at the local r location, but also depends on the value at other r locations (as denoted by the star signs).

The integro-differential equation that describes the Vlasov-Poission system is thus obtained by substituting Eq. (16) into Eq. (5). It is important to note that the solution of such a system depends only on five independent dimensionless parameters (δ_i, δ_p, φ_p, ρ_p, β), and yet it is independent of the mass ratio $\mu_i = m_i/m_e$.

To solve this integro-differential equation numerically, a non-uniform mesh for the spatial coordinate r is created and truncated at a maximum radius r_{max}. The values of the potential $\varphi(r)$ and density $n_\alpha(r)$ at all mesh points are contained inside two vectors $\boldsymbol{\varphi}$ and $\boldsymbol{n}_\alpha$. With an initial guess for $\boldsymbol{\varphi}$, the numerical scheme first computes the densities $\boldsymbol{n}_\alpha$ with Eq. (16) by carrying out the integrals numerically with Simpson's rule (as a Vlasov solver). Then, by using a finite-element formulation [12, 13], with the boundary conditions for a cylindrical probe as $\varphi|_{r=1} = \varphi_p$ and $\mathrm{d}\varphi/\,\mathrm{d}r|_{r_{max}} = -\varphi/r|_{r_{max}}$ [14], a Poisson solver for Eq. (5) calculates a new $\boldsymbol{\varphi}_{out}$ from the $\boldsymbol{n}_\alpha$ previously obtained. These two steps are the main building blocks of the Newton-Raphson iterative scheme that solves the non-linear algebraic equation $\boldsymbol{F}(\boldsymbol{\varphi}) = \boldsymbol{\varphi} - \boldsymbol{\varphi}_{out} = \boldsymbol{0}$. The most costly part of the algorithm is to numerically calculate the Jacobian for $\boldsymbol{F}$, which is carried out by several processors in parallel.

3. Current-voltage characteristics

Once $\varphi(r)$ is found, the current per unit probe length (normalized to the electron random thermal current I_{the}) can be found as

$$i_\alpha \equiv \frac{I_\alpha}{I_{the}} = \frac{2G_\alpha}{\sqrt{\pi}} \int_{u_\alpha^*}^{\infty} l_\alpha^*(\epsilon_\alpha) \exp(-\epsilon_\alpha)\, \mathrm{d}\epsilon_\alpha \ , \quad I_{the} = 2\pi R_p e N_\infty \sqrt{\frac{k_B T_e}{2\pi m_e}} \tag{17}$$

$$G_i = -\sqrt{\delta_i/\mu_i}, \quad G_e = 1, \quad G_{em} = -2\beta\sqrt{\delta_p} \ ,$$

being invariant with r and positive for collected electron current. For a set of independent parameters (ρ_p, μ_i, δ_i, δ_p, β), the current-voltage characteristic ($i_t = i_e + i_i + i_{em}$ versus φ_p) can be obtained by varying the probe bias φ_p.

Based on the self-consistent full-kinetic model, the first results on the current-voltage characteristics were presented in [9] for an EP with radius $R_p \approx 3.6\,\mathrm{mm}$ and immersed in an oxygen plasma with $T_i = T_e \approx 0.25\mathrm{eV}$ and $N_\infty \approx 1.07 \times 10^{12}\,\mathrm{m}^{-3}$. Together with the material thermionic properties $W \approx 2.5\mathrm{eV}$ and $\lambda_{RD} = 1$, the IV curves for different probe temperature T_p were calculated. Non-monotonic potential due to space-charge effects were successfully captured. This non-monotonic behaviour is not only present when the probe is negatively biased relative to the plasma ($\varphi_p < 0$), but also extends to positive probe bias ($\varphi_p > 0$). The higher the emission level is, this non-monotonic regime covers a larger range of φ_p. In this work, we consider the same ambient parameters as $\delta_i = 1$, $\mu_i = 29164.1$, $\delta_p = 0.32$, and $\beta = 1.716$, but varying the probe radius from $\rho_p = 0.1$ to $\rho_p = 2$ [see Fig. 1].

For a very negative probe bias ($\varphi_p \ll 0$), the probe emits electrons following the RD law, being invariant with φ_p. Because this emitted electron current is much larger than both the plasma ion current and the plasma electron current, the total current is also invariant with φ_p. The numerical results for such φ_p range can be found in [9]. Although not shown in Fig. 1, the IV curves for different ρ_p overlap with each other, as a result of normalizing the current with the thermal electron current. For a very large probe bias ($\varphi_p \gg 0$), the probe collects mainly electron current. This dimensionless current can depend on ρ_p if the probe collects electrons beyond the Orbital-Motion-Limited (OML) regime [11]. Nevertheless, numerical results are not shown for this φ_p range since it is not relevant for the purpose of this work.

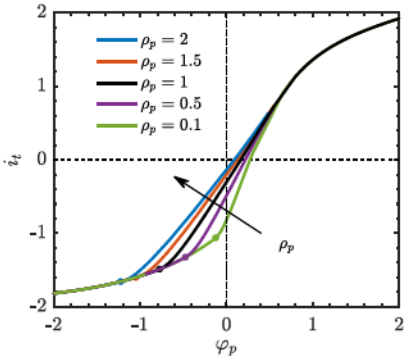

Figure 1. Current-voltage characteristics for different probe radius ρ_p, with $\delta_i = 1$, $\mu_i = 29164.1$, $\delta_p = 0.32$, and $\beta = 1.716$.

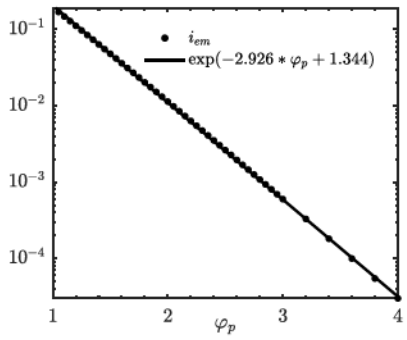

Figure 2. The calculated and fitted emitted electron current i_{em}, in the case of $\varphi_p > 0$ and monotonic potential profile ($\rho_p = 0.1$).

In Fig. 1, numerical results are presented for φ_p values that are close to zero. For negative probe bias ($\varphi_p < 0$), a dotted marker is placed on each curve to indicate the transition between

the monotonic and non-monotonic regime. To the left of the transition point, the potential profile is monotonic. It can be observed that, as long as within the monotonic regime, all curves overlap with each other. Nevertheless, the net current no longer follows the RD law as being a constant value. It increases because the current from the plasma species becomes comparable with the emitted electron current. To the right of the transition point, the potential profile becomes no-monotonic and the emitted electron current is substantially reduced by the virtual cathode in front of the probe. The net current (positive for electron collection) thus rises rapidly and deviates from the overlapped route. For a larger probe radius, a larger net current implies more reduction of the emitted electron current, thus a stronger space-charge effect.

In the case of positive probe biases ($\varphi_p > 0$), for all the curves in Fig. 1, the non-monotonic potential profile persists for some positive probe biases ($\varphi_p > 0$). Because the RD current is larger than the random thermal current ($I_{RD}/I_{th} \approx 1.94$), the floating (zero-net-current) condition occurs at a positive probe bias. For $\varphi_p > 0$, the interest here is the emitted electron current [15]. This problem was first tackled by Langmuir. The electron current in *vacuum* was calculated considering electrons emitted from an internal cylindrical anode to an external coaxial cathodic cylinder, see Fig. 40 in [16]. According to the results from Langmuir, if i_{em} is plotted against φ_p with natural logarithm scale and linear scale respectively, the slope is estimated to be $1/\delta_p$. Our numerical calculations show that, as long as the potential profile is monotonic, i_{em} is identical for different ρ_p. In Fig. 2, the emitted electron current i_{em} (the dotted curve) for $\rho_p = 0.1$ is plotted (in decimal logarithm scale) versus φ_p (in linear scale). The value of i_{em} decreases exponentially, as indicated by the linear slope in this plot. After applying an exponential fitting (the solid line), the slope of the decreasing i_{em} in a natural logarithm scale is found to be 2.93, close to $1/\delta_p \approx 3.13$. The slight difference could result from the presence of plasma particles, which modifies the potential profile and thus the current.

3.1. Inflection-point method

The inflection point method makes use of the derivatives of the IV characteristics ($\mathrm{d}i_t/\mathrm{d}\varphi_p$) to measure the plasma potential. In [17], it is stated that, if an emissive probe is operated at sufficiently low emission level to minimize space-charge effects, the probe bias - at which the maximum of the derivatives occurs - is equal to the plasma potential. The inflection point refers to this maximum of the derivatives. Based on this theoretical prediction, in experiments, the inflection points are first measured for a number of low emission levels and then linearly extrapolated to obtain the inflection point for zero emission. Therefore, the plasma potential is given by the probe potential that coincides with this extrapolated inflection point in the limit of zero emission. The justification of this method has been provided qualitatively in [17] and quantitatively based on a model assuming planer emitter, cylindrical collector, and cold emitted electrons [15][18]. Before the attempts to seek for the justification by taking derivatives of the IV curves from numerical calculations, analytical results for zero emission can already provide significant insights.

If there is no emission ($\beta = 0$) and the probe is biased at the plasma potential ($\varphi_p = 0$), we first assume that there is no electric field anywhere and the plasma is directly connected to the probe without a sheath region. It can be proved later that such a flat potential is indeed a self-consistent solution of the Vlasov-Poisson system. In this case, there is no electric potential barrier that repels the plasma particles: $u^*_\alpha = u^*_{\alpha r} = u_{\alpha r} = 0$. Electrons and ions move towards the probe due to orbital effects alone. According to Eq. (13), the angular momentum limitation for the *non-forbidden* condition is given by ${l_{\alpha r}}^2 = r^2\epsilon_\alpha$. Because it decreases all the way towards the probe, we have the *sufficient* condition as $l^*_{\alpha r} = l_{\alpha r} = r\sqrt{\epsilon_\alpha}$ at every r. Consequently, the *captured* condition for the particles to be collected by the probe is determined by the *non-forbidden* condition at the probe only, i.e., $u^*_\alpha = u_{\alpha r}(r = 1)$ and $l^*_\alpha = l_{\alpha r}(r = 1)$. The current is then said to be orbital-motion-limited (OML) [19] [11]. Substituting $u^*_\alpha = 0$ and $l^*_\alpha = \sqrt{\epsilon_\alpha}$ into

Eq. (17), the currents are given by

$$i_i = -\sqrt{\delta_i/\mu_i}\ , \quad i_e = 1\ , \quad i_t = 1 - \sqrt{\delta_i/\mu_i}\ , \tag{18}$$

which coincide with the random thermal currents.

To prove that the flat potential profile is a self-consistent solution for a non-emitting probe biased at the plasma potential, the particle densities need to be found. By substituting $l^*_{\alpha r} = r\sqrt{\epsilon_\alpha}$ and $u^*_{\alpha r} = 0$ into Eq. (12), the electron and ion densities are given by [19]

$$n_i = n_e = 1 - \frac{\arcsin(1/r)}{\pi}\ , \tag{19}$$

which recovers the classical OML result with the particle density at the probe being 1/2. Equation (19) has been used as an initial condition in the analytical studies and the numerical simulations for transient effects [20] [21]. The reason for this normalized density to be less than one everywhere (i.e., particle density smaller than the plasma density) can be explained by Fig. 7 in [22]. Due to the particles that are captured by the probe, they do not turn back to the plasma, which results in a non-populated region in the distribution function for out-going particle populations. This non-populated region grows towards the probe. Because the particles arriving at the probe surface are collected by the probe (with no out-going particle populations), the distribution function becomes half-Maxwellian at the probe (thus $n_\alpha = 1/2$ under OML condition). According to Eq. (19), the net charge density is zero everywhere. Therefore, given by Poisson's equation, the flat potential profile is a self-consistent solution for $\varphi_p = 0$.

To determine the IV derivative near the plasma potential, it requires the expression for the net current i_t at the vicinity of $\varphi_p = 0$. It has been shown in the previous paragraphs that, if the probe is biased at the plasma potential ($\varphi_p = 0$), both ions and electrons currents do not only coincide with the thermal currents but also with the OML currents. Therefore, at the vicinity of $\varphi_p = 0$, the current for the attracted species can be expected to follow the OML law, which is confirmed by the numerical results [9][22]. For repelled species, the collection is also OML as the *captured* condition is determined by the *non-forbidden* condition at the probe only. Nevertheless, the electric potential barrier at the probe ($u^*_\alpha > 0$) leads to the Boltzman current law. By applying $u^*_\alpha = 0$ for attracted species, $u^*_\alpha = u_{\alpha r}(r = 1)$ for repelled species, and $l^*_\alpha = \sqrt{\epsilon_\alpha + u_{\alpha r}(r = 1)}$ for both, the currents at the vicinity of $\varphi_p = 0$ are exactly given by

$$\varphi_p < 0: \quad i_{e-} = \exp(\varphi_p)\ , \quad i_{i-} = -\sqrt{\delta_i/\mu_i}\left[\mathrm{erfcx}\left(\sqrt{-\varphi_p/\delta_i}\right) + 2\sqrt{-\varphi_p/(\pi\delta_i)}\right]\ , \tag{20}$$

$$\varphi_p > 0: \quad i_{e+} = \mathrm{erfcx}\left(\sqrt{\varphi_p}\right) + 2\sqrt{\varphi_p/\pi}\ , \qquad i_{i+} = -\sqrt{\delta_i/\mu_i}\exp(-\varphi_p/\delta_i)\ . \tag{21}$$

The derivatives of $i_{t-} = i_{e-} + i_{i-}$ and $i_{t+} = i_{e+} + i_{i+}$ are thus given by

$$\frac{\partial i_{t-}}{\partial \varphi_p} = \exp(\varphi_p) + \frac{\mathrm{erfcx}\left(\sqrt{-\varphi_p/\delta_i}\right)}{\sqrt{\delta_i\mu_i}}, \quad \frac{\partial i_{t+}}{\partial \varphi_p} = \mathrm{erfcx}\left(\sqrt{\varphi_p}\right) + \frac{\exp(-\varphi_p/\delta_i)}{\sqrt{\delta_i\mu_i}}\ . \tag{22}$$

For two different cases, the total current and the derivatives are plotted in Fig. 3. The inflection point of the IV curve (as the maximum of the derivative curve) at $\varphi_p = 0$ can be observed. Note that, due to $\mathrm{d}\ \mathrm{erfcx}(\sqrt{x})/\mathrm{d}\ x = \mathrm{erfcx}(\sqrt{x}) - 1/\sqrt{\pi x}$, the second derivative of the IV curve becomes to be positive infinity to the left of $\varphi_p = 0$ and negative infinity to the right.

As previously demonstrated, a flat-potential is a self-consistent solution for a non-emitting probe biased at the plasma potential. Since a flat potential requires an equal density of plasma ion and plasma electron everywhere [see Eqs. (5) and (19)], the presence of emitted electrons would thus violate this zero net charge and, according to Poisson's equation, a sheath region with non-zero electric field would build up. It can then be concluded that a flat potential can not be possible for an emissive probe biased at the plasma potential.

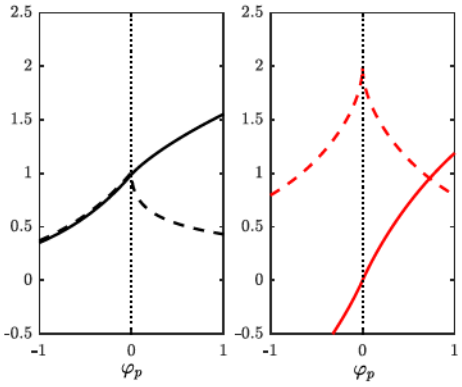

Figure 3. The i_t-versus-φ_p curve (solid curve) and the $\mathrm{d}i_t/\mathrm{d}\varphi_p$ derivative (dashed curve) near $\varphi_p = 0$ for two cases: $\delta_i = 1$ and $\mu_i = 1$ (left); $\delta_i = 1$ and $\mu_i = 10000$ (right).

4. Floating-potential characteristics

The probe is said to be floating if the net current is zero ($i_t = 0$). In laboratories, an emissive probe is heated to different temperatures (δ_p) to achieve different emission levels (β). The probe bias at the floating condition - the floating potential ($\varphi_f = e\phi_f/kT_e$) - is measured. The FP characteristics can thus be obtained by plotting φ_f versus δ_p (or versus other quantities that are equivalent to emission level, such as RD current and heating current). Such a FP curve was first shown by Kemp and Sellen, which rises rapidly at low emission and plateaus at high emission [6]. They claim that the knee (or break point) of this curve approximates the plasma potential. In 1967, by considering planar geometry and fluid approximation, Hobbs and Wesson found the monotonic to non-monotonic transition on a FP curve. The probe-to-plasma potential at that transition was found to be $e\phi_p \approx -k_B T_e$ (i.e., $\varphi_p \approx -1$) [3]. Since then, the floating-potential method is said to underestimate the plasma potential with an error being close to the electron temperature T_e.

To calculate this FP characteristic (φ_p versus δ_p), our numerical scheme is modified. The vector function $\boldsymbol{F} = \boldsymbol{0}$ (solved by the Newton-Raphson iterative scheme) considers the floating probe bias φ_f and the floating condition $i_t = 0$ as an additional unknown and an additional equation, respectively. The parameters that determine the FP characteristics are (ρ_p, μ_i, δ_i, δ_s, δ_w). The emission level β (a parameter in the Vlasov-Poisson system) is determined by δ_w and δ_s as given in Eq. (7).

In this work, the parameter set is first chosen as $\rho_p = 1$, $\mu_i = 29164.1$, $\delta_i = 1$, $\delta_w = 10$, and $\delta_s = 2 \times 10^{-10}$. The FP characteristics are then compared by varying one of the parameters as shown in Figs. 4-6. The probe is found to be able to float at positive probe bias ($\varphi_f > 0$), in agreement with the PIC simulation for planar geometry [5]. The saturated behaviour of the floating potential at high emission level is not observed for the parameters presented in this work. Such a non-saturating behaviour has also been found by PIC simulations for spheres [23] and in experiments performed for the plasma jet system [24]. For this reason, the knee of the FP curve is adopted in this work to evaluate the accuracy of floating-potential method. The knee is shown in Figs. 4-6 by a dot marker on each FP curve. To define this knee without ambiguity, it has been taken as the transition between non-monotonic and monotonic potential profile. That is to say, on each FP curve, to the left of the knee, the potential profile is monotonic (due to less emission), otherwise non-monotonic. If the knee occurs at $\varphi_f = 0$, the floating-potential method estimates the plasma potential precisely. If the knee occurs at $\varphi_f < 0$, the floating-potential method underestimates the plasma potential with the error being $|\varphi_f|$. What we are interested here is to see how this error varies with the ambient condition.

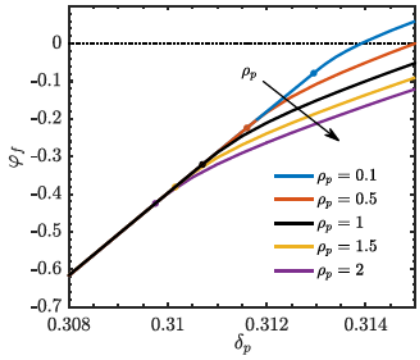

Figure 4. The floating-potential characteristics for different ρ_p.

The probe radius ρ_p is varied between 0.1 and 2, as shown in Fig. 4. The values of φ_f at the knee lie between 0 and -1, thus underestimating the plasma potential. They are also found to decrease with the probe radius. Nevertheless, this decreasing behaviour seems to weaken at larger radius as the curves become closer to each other. Although further calculations still need to be carried out to fully recover the planar solution $\varphi_f \approx -1$ for $\rho_p \gg 1$, this asymptotic behaviour suggests that this is viable. We can also say that, the smaller the probe radius is, the knee is closer to the plasma bias. Therefore, for a better approximation of the plasma potential using floating-potential method, a smaller probe radius is preferred.

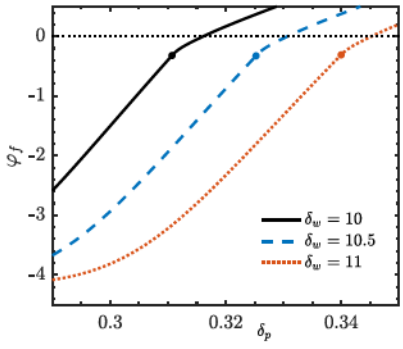

Figure 5. The floating-potential characteristics for different δ_w.

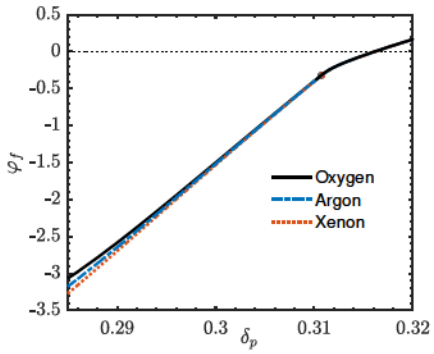

Figure 6. The floating-potential characteristics for different ion mass.

If the work function of the emitting material (δ_w) is reduced, the emission level (β) would increase according to Eq. (7). This noticeably modifies the floating-potential characteristics as shown in Fig. 5. If we look at the curves at a same probe temperature (δ_p), for a lower work function (δ_w), the floating potential (φ_f) increases due to higher emission level (β). Such a rise in φ_f serves to repel the excess of emitted electrons back to the probe and thus to attain the zero-net-current condition. Nevertheless, the influence of δ_w on φ_f weakens as δ_p decreases. This is because, for $\delta_p \ll \delta_w$, the change of the emission level β is dominated by δ_p other than δ_w [see Eq. (7)]. Although not shown in this figure, these three curves are superimposed at very low δ_p values, in that the floating potential is mainly determined by the plasma electron and ion current. At the end, since the knee is found to vary little with δ_w, the accuracy of the floating-potential method is the same for different materials.

Calculations were also carried out for Xenon and Argon [see Fig. 6]. Three curves are found to overlap with each other near the knee and for higher δ_p values, yet deviate from each other for low δ_p values. This results from the same reason mentioned in the paragraph above. Since the decrease in δ_p reduces the emission level β, the ion current becomes comparable to (or even can be larger than) the RD current. Under these circumstances, the floating potential would vary with the plasma-ion properties (such as ion mass) due to their influences on the ion current. If the ion mass is increased, the ion current tends to reduce. Therefore, to balance the plasma electron current and thus to retain the zero-net-current condition, the probe needs to float at a more negative potential to collect more ions, as shown by the dotted curve for Xenon. If the probe temperature δ_p increases, the floating potential also increases. When it becomes close to the plasma potential, as in the case of the knee in Fig. 6, the ion current becomes negligible compared to the emitted electron current. The influence of the ion properties on the knee thus becomes negligible and the knee is found to be independent on the ion mass. Due to this reason, calculations for different δ_i would not provide more information.

5. Conclusions

Based on the Orbital Motion Theory, a full-kinetic model for emissive probes with two-dimensional cylindrical geometry can solve the Vlasov-Poisson system self-consistently and determine the potential and density profiles for arbitrary plasma parameters (as long as the effects of collisions, plasma drift, particle trapping, transient effects, and magnetic fields are negligible) [9]. Such a model can capture the kinetic nature of the plasma sheath, reveal the non-negligible space-charge effects, solve for the non-monotonic potential profile without ambiguity, and unify both collecting (Langmuir) [19] and emissive probes in one compact framework. Some hypotheses for the numerical calculations presented this work can be easily relaxed within the framework of the model [22]: 1) the distribution function of the plasma and emitted species can be substituted by any energy distribution; 2) trapped particles can be included with a prescribed distribution function (under the condition of axial-symmetric electric field); 3) multiple plasma or emitted species, with arbitrary charge number (negative and positive), can be included.

Based on the numerical results, extensive parametric studies can be used to asses the accuracy of plasma-potential measurements using emissive-probe techniques. For the parameter range presented in this work, it is found that: (a) the space-charge effect increases with probe radius; (b) for a positive probe bias (relative to the plasma potential) and a monotonic radial potential profile, the emitted electron current decreases exponentially with the probe bias and the slope in the semi-natural-logarithmic plot is approximately $1/T_p$; (c) the probe can float at a positive bias relative to the plasma; (d) to determine the plasma potential using the knee of the floating-potential curve, a smaller probe radius is preferred; (e) the reliability of the floating-potential method is not influenced by the work function of the emitting material, neither the plasma-ion properties. An appropriate fitting of experimental EP measurements to this numerically calculated results can also be used to predict other plasma parameters, in addition to the plasma potential. Besides probe theory and plasma diagnostics, the numerical results can also benefit space applications such as spacecraft charging [25] and Low Work function Tethers (LWTs) for space debris removal [26].

To investigate the inflection-point method, analytical analysis for zero-emission was carried out, in the purpose to determine the current and its derivative for the probe bias at the vicinity of the plasma potential. Inflection point occurs exactly at the plasma potential, yet with the second derivative being infinite. In addition, for a non-emitting probe biased at the plasma potential, a flat potential is found to be a self-consistent solution of the Vlasov-Poisson system. In this case, the density of each species decreases towards the probe, yet with the net charge density being zero everywhere. If there is emission, emitted electrons result in negative space charge and a flat-potential solution is thus not self-consistent for an emissive probe biased at

the plasma potential.

Acknowledgments

This work was supported by the Ministerio de Economía y Competitividad of Spain (Grant No ESP-2016-75887). Work by G. Snchez-Arriaga was supported by the Ministerio de Economía y Competitividad of Spain (Grant No RYC-2014-15357).

References

[1] Ionita C, Grnwald J, Maszl C, Starz R, Cercek M, Fonda B, Gyergyek T, Filipic G, Kovacic J, Silva C, Figueiredo H, Windisch T, Grulke O, Klinger T and Schrittwieser R 2011 *Contrib. Plasma Phys.* **51** 264–270

[2] Sheehan J P, Raitses Y, Hershkowitz N and McDonald M 2017 *J. Propul. Power* **33** 614–637

[3] Hobbs G D and Wesson J A 1967 *Plasma Physics* **9** 85

[4] Takamura S, Ohno N, Ye M and Kuwabara T 2004 *Contrib. Plasma Phys.* **44** 126–137

[5] Campanell M D and Umansky M V 2016 *Phys. Rev. Lett.* **116** 085003

[6] Kemp R F and Sellen J M 1966 *Rev. Sci. Instrum.* **37** 455–461

[7] Chang K W and Bienkowski G K 1970 *Phys. Fluids* **13** 902–920

[8] Schuss J J and Parker R R 1974 *J. Appl. Phys.* **45** 4778–4783

[9] Chen X and Sanchez-Arriaga G 2017 *Phys. Plasmas* **24** 023504

[10] Richardson O W 1916 *The emission of electricity from hot bodies* (Longmans, Green and co.)

[11] Sanmartin J R and Estes R D 1999 *Phys. Plasmas* **6** 395–405

[12] Choiniere E 2004 *Theory and experimental evaluation of a consistent steady-state kinetic model for 2-D conductive structures in ionospheric plasmas with application to bare electrodynamic tethers in space* Ph.D. thesis Univ. of Michigan

[13] Sanchez-Arriaga G and Sanmartin J R 2012 *Phys. Plasmas* **19** 063506

[14] Bernstein I B and Rabinowitz I N 1959 *Phys. Fluids* **2** 112–121

[15] Sheehan J P and Hershkowitz N 2011 *Plasma Sources Sci. Technol.* **20** 063001

[16] Langmuir I and Compton K T 1931 *Rev. Mod. Phys.* **3** 191–257

[17] Smith J R, Hershkowitz N and Coakley P 1979 *Rev. Sci. Instrum.* **50** 210–218

[18] Ye M Y and Takamura S 2000 *Phys. Plasmas* **7** 3457–3463

[19] Laframboise J G 1966 Theory of spherical and cylindrical langmuir probes in a collisionless, maxwellian plasma at rest Tech. rep. University of Toronto Institute for Aerospace Studies UTIAS Report, No. 100

[20] Sanmartin J R 1972 *Phys. Fluids* **15** 391–401

[21] Sanchez-Arriaga G 2013 *Phys. Plasmas* **20** 013504

[22] Chen X and Sanchez-Arriaga G 2017 *Phys. Plasmas* **24** 103515

[23] Delzanno G L and Tang X Z 2014 *Phys. Rev. Lett.* **113** 035002

[24] Marek A, Jlek M, Pickov I, Kudrna P, Tich M, Schrittwieser R and Ionita C 2008 *Contrib. Plasma Phys.* **48** 491–496

[25] Thiebault B, Hilgers A, Sasot E, Laakso H, Escoubet P, Genot V and Forest J 2004 *J. Geophys. Res. A* **109** A12207

[26] Sanchez-Arriaga G and Chen X *J. Propul. Power* Advance online publication. doi:10.2514/1.B36561